Received: 23 February 2023 | Revised: 15 May 2023 | Accepted: 22 May 2023

DOI: 10.1002/pol.20230109

RESEARCH ARTICLE

JOURNAL OF POLYMER SCIENCE WILEY

The weathering resistance of quaternary High-density polyethylene (HDPE) composites: Effects of weld lines, formulation and degradation on tensile properties

David Viljoen[1,2] | **Johan Labuschagné**[2] | **Ines Kuehnert**[1]

[1]Polymer Processing Department, Leibniz-Institut für Polymerforschung Dresden e.V., Dresden, Germany

[2]Department of Chemical Engineering, Institute of Applied Materials, University of Pretoria, Pretoria, South Africa

Correspondence
Johan Labuschagné, Department of Chemical Engineering, Institute of Applied Materials, University of Pretoria, Hatfield, Pretoria 0002, South Africa.
Email: johan.labuschagne@up.ac.za

Funding information
Technology and Human Resources for Industry Programme (THRIP), Grant/Award Number: THRIP/133/31/03/2016

Abstract

In this work, the effects of weld lines, additives and the degree of QUV weathering on the tensile behavior of a range of high-density polyethylene composites with calcium carbonate, stabilizers and a carbon black/SEBS masterbatch are studied. The degree of weathering is characterized using FTIR-derived carbonyl, double-bond and carbonate indexes based on curve fitting, to allow for the fairer comparison of specimens with and without calcium carbonate. Weld-line specimens exhibited more rapid degradation than that seen in the reference specimens, while the exposed surfaces of the specimens degraded more quickly than the unexposed surfaces. ISO G154 Cycle 1 and Cycle 6 weathering protocols were compared. The additives were found to be effective at decreasing oxidative degradation, albeit with reduced effects at higher loadings and in mixed systems. These findings were mirrored in the mechanical properties of the specimens, with the modified specimens even exhibiting broadly improved properties with increasing aging. Elongation at break was most sensitive to weathering, with increasing degradation with increasing weathering across almost all specimens.

KEYWORDS

calcium carbonate, carbon black, high-density polyethylene, hindered-amine light stabilizer, QUV, tensile testing, weathering stability, weld lines

1 | INTRODUCTION

A key consideration in the specification of polymers, particularly for outdoor use, is their resistance to weathering. While it would be ideal to study this in a natural environment, this is frequently slow and subject to unexplained variance. As a result, accelerated weathering is used—for example through the use of a QUV. This is known to deviate from natural weathering in unpredictable ways, but serves as an efficient and effective method for the comparison of formulations.

High-density polyethylene (HDPE) is among the most frequently used commodity polymers, including for outdoor applications, owing to its low cost, acceptable mechanical properties and chemical resistance, as well as the great improvements that can be made to its weathering resistance through the judicious use of additives.[1] As with many polymers, it is subject to oxidation through an auto-oxidative pathway[2] (which differs somewhat from that originally proposed by Bolland, Gee and coworkers for rubber and lipids[3–5]). Impurities such as catalyst residues may initiate the

process.[6,7] This may be accelerated through exposure to heat and (UV) light[2] as well as moisture/humidity.[8]

Several approaches may be taken to counteract this degradation. The first is chemical stabilization, whereby additives are used to interfere in the auto-oxidative cycle of the material. These additives may take the form of primary antioxidants, secondary antioxidants or hindered-amine light stabilizers, among others.

Further, additives may be used to absorb or block the light that may accelerate the auto-oxidation. It may also be found that these additives act in synergy with the stabilizers to greatly improve the weathering resistance of the materials.[9] Among these additives is carbon black, a highly absorbing particulate additive that may, depending on its surface chemistry, offer particularly strong synergies with stabilizers. It is frequently required that nanoscale additives of the type of carbon black are introduced in the form of masterbatches, wherein the additive is carried at high loading in a polymer matrix, for dust mitigation and more facile processing.[10]

Other additives may also be used in HDPE, with the largest volume of these consisting of fillers—used to replace some of the polyolefin matrix for cost and environmental reasons, and to alter the mechanical behavior and appearance of the resulting composite.[11] Most common among these is calcium carbonate. This filler is known for its low cost, tailorability (through type, particle size and compatibilization) and the mechanical improvements that it may bring.[11] By obstructing UV radiation, it may also offer improvements in weathering resistance.[12,13]

Weld lines result from impinging melt fronts, typical in injection molding, and serve as a major structural defect.[14,15] These may take the form of "cold" welds, where the melt fronts meet in a stationary plane, or "hot" welds, where the melt fronts flow together after meeting. V-notches frequently accompany (cold) weld lines, resulting from air trapped by the impinging melt fronts, and serve as natural initiation points for mechanical failure. In polypropylene, specimens with weld lines have been found to exhibit similar degradation of their mechanical properties to that seen in specimens without weld lines, albeit with weaker properties overall.[16]

Natural and accelerated weathering is used to characterize the weathering resistance of specimens. Accelerated weathering, such as that using a QUV, makes use of cycles of increased temperature, radiation and humidity in an effort to dramatically speed up the degradation of test specimens.

Fourier-transform infrared spectroscopy (FTIR), specifically attenuated total reflectance Fourier-transform infrared spectroscopy (ATR-FTIR), may be used to study changes in the chemical groups near the surfaces of specimens. Common is the use of a carbonyl index to monitor the oxidative degradation of a specimen.[17] A double-bond index is also sometimes used,[18] to monitor the formation of unsaturations that may play a critical part in the auto-oxidative degradation of these materials.[2]

In this work, it is sought to gain a better understanding of the interplay of the additives, weathering type and duration, and weld lines on the oxidative degradation of the materials. This is investigated through monitoring of the chemical changes in the material with weathering in terms of carbonyl, double-bond and carbonate indexes. Subsequently, the tensile behavior of specimens of these materials was investigated as a function of additives, degree of aging/oxidation and the presence of weld lines.

2 | EXPERIMENTS

2.1 | Materials

Commercial, food-safe materials were used in this study, consisting of an injection-molding grade of HDPE (Dow HDPE 25055E, Midland, MI, USA), surface-coated, ultrafine natural calcium carbonate with a mean particle size of 0.8 μm (OMYA Hydrocarb 95 T-OG, Oftringen, Switzerland), a stabilizer package of a constant 3:2 ratio of BASF (Rhineland-Palatinate, Germany) Chimassorb 944 and BASF Irgafos 168 and a carbon black masterbatch (Caparol NEFA MB F 21504 Schwarz, Ober-Ramstadt, Germany). The masterbatch consists of 28% of a furnace black with an average particle size of 16 nm (Orion Engineered Carbons Printex F 80, Luxembourg) in a thermoplastic elastomer (SEBS) matrix. These components will henceforth be referred to as HDPE, CC, S and CB.

The materials were combined based on a D- and I-optimal experimental design for a quadratic linear model with interactive terms, while some duplicate and additional points were added for checks of the quality of the models. These materials form part of the same broader study as other works by Viljoen, Labuschagné et al.[15,19] The formulations used are outlined in Figure 1 and Table 1.

2.2 | Processing

Compounding was performed on a Krauss Maffei Berstorff (Hannover, Germany) ZE 25-Cl with a 1200 mm (48 D) screw. The temperature profile was set to increase from 220°C at the main feed to 235°C at the die. Side feeds were available at approximately 14 D and 25 D, with CC introduced through one or both of these as outlined in Table 1. The 60CC materials saw equal amounts of CC introduced through each side feed. The extrudate was cooled in a water bath and pelletized.

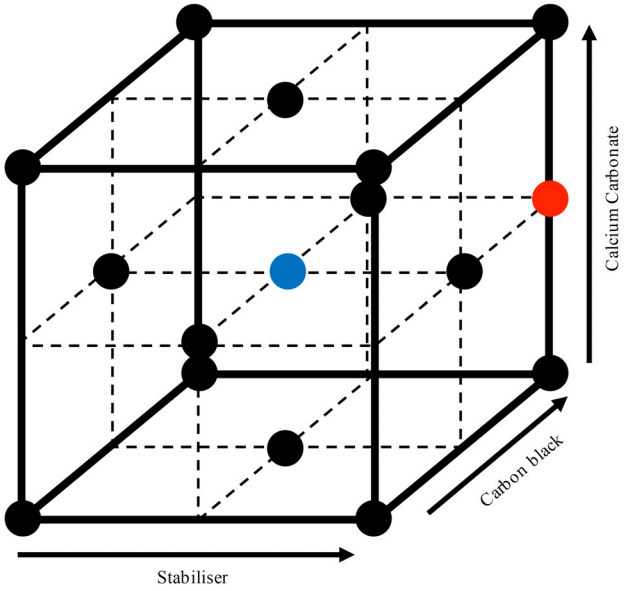

FIGURE 1 Slack-variable representation of experimental design. Reproduced with permission from Viljoen and Labuschagné, Polymer Testing; published by Elsevier, 2020.[15,19]

TABLE 1 Experimental design: formulations and feed points. Reproduced with permission from Viljoen and Labuschagné, Polymer Testing; published by Elsevier, 2020.[15,19]

	Component (%)				CC feed	
Formulation	HDPE	CC	CB	S	1	2
01	65.90	30	3.60	0.50		•
02	65.90	30	3.60	0.50	•	
03	99.50	0	0	0.50		
04	100.00	0	0	0		
05	97.95	0	1.80	0.25		
06	95.90	0	3.60	0.50		
07	96.40	0	3.60	0		
08	69.75	30	0	0.25		•
09	67.70	30	1.80	0.50		•
10	67.95	30	1.80	0.25		•
11	67.95	30	1.80	0.25		•
12	68.20	30	1.80	0		•
13	66.15	30	3.60	0.25		•
14	39.50	60	0.00	0.50	•	•
15	40.00	60	0	0	•	•
16	37.95	60	1.80	0.25	•	•
17	35.90	60	3.60	0.50	•	•
18	36.40	60	3.60	0.00	•	•

The resulting granules were held overnight in 80°C vacuum ovens, prior to injection molding. An Arburg (Loßburg, Germany) Allrounder 420 C 1000–250 was used for injection molding, configured with a cycle time of 30 s, a barrel temperature profile of 40/210/200/210/220/230/230°C, a melt temperature of 220°C and a mold temperature of 50°C. Dedicated molds were used to produce the weld-line (WL) and reference (REF) specimens, making use of an ISO 527-2 1BA geometry and lengthwise injection. A linear injection flow rate of 40 mm/s was used with a peak injection pressure of 190 bar and a holding pressure of 78 bar. For high-quality specimens to be produced, subtle adjustments were made to the pressure profiles of the formulations.

2.3 | Weathering

Weathering was performed in a Q-Lab QUV/se accelerated weathering tester, according to ISO G154 Cycle 1 and Cycle 6 (denoted henceforth C1 and C6), in an attempt to determine the effect of radiation intensity on the degradation of the specimens. The weathering times are outlined in Table 2, with the "Max" level of weathering equal to 1212 h of C1 and 1212 h of C6. This level was the result of leaving the relevant specimens in the system for the 408 and 804 h aging steps of the C1 and C6 levels.

2.4 | Characterization

FTIR analyses were performed using a Bruker (Massachsetts, USA) Tensor 27 with a Pike "MIRacle" ATR unit with a diamond crystal. A resolution of 4 cm^{-1} was used over 16 scans.

Tensile tests were performed using a Zwick/Roell Z2.5 universal testing machine (ZwickRoell GmbH & Co. KG, Ulm, Germany) with a Zwick/Roell pneumatic sample holder. The modulus of the specimens was determined between strains of 0.05% and 0.25% at a strain rate of 1 mm/min. After this, the remaining mechanical characteristics were determined at a strain rate of 50 mm/min. The first specimen of an aging level/specimen type/material combination was always extended until failure. In the event of very ductile materials (Formulation 3 to Formulation 7) the subsequent specimens had their elongation halted at 10 mm of strain for the sake of time. The specimens of other materials were always extended until failure. As many specimens as available were tested in this manner, with a minimum of three per combination of aging, specimen type and formulation.

2.5 | Statistical analysis

All independent variables were normalized, according to Equation (1). This allows, first, discussion based on a natural reference point of unaged specimens of the virgin

TABLE 2 Weathering exposures for REF and WL specimens.

Weathering	REF	WL
204 h C1	•	
408 h C1	•	
804 h C1	•	
408 h C6	•	•
804 h C6	•	•
Max	•	•

HDPE and, second, more balanced comparison of effects based on observation as applied rather than scaling based on the potency of the compounds, where, for example, S would have an outsized impact.

$$X_n = \frac{X}{\max(X) - \min(X)} \quad (1)$$

A Frequentist approach was taken. The t-tests used outside of parameter significance in this work, for example in comparing FCI and BCI, are standard dependent t-tests for paired samples. When used in this way, the unaged specimens are omitted unless otherwise noted, as the front and back surfaces are assigned at the start of aging.

Model fits were performed using linear regression in the statsmodels module (version 0.12.1)[20] of a MacOS 12.6 installation of Python 3.8.12. Peak finding was performed using proprietary code based on the method by Fleißner et al.[21] in the same Python environment, built on the NumPy (version 1.19.2)[22] and SciPy (version 1.5.2) packages.[23]

3 | RESULTS

3.1 | FTIR characterization

First, it was sought to gain an overarching understanding of the peaks present in the FTIR data, in terms of their position and, then, likely chemical origin. In Figure 2 is presented a histogram summarizing the results of algorithmically determining the presence of peaks in the range 1500 to 1850 cm^{-1}. This was performed by, first, taking the fourth derivative of an FTIR curve,[21] after which peak identification is performed based on simple comparison with neighboring values and subject to various conditions relating to separation of peaks (minimum peak separation of 2.5 cm^{-1}) and prominence (minimum of 5% of the maximum height).

Based on Figure 2, it is clear that a multitude of peaks may be found—owing, at least in part, to noise in the data and the fourth-derivative method employed. Peak finding may then again be performed, with an eye to identifying the most significant peaks. Based on this, with a minimum distance of 6 cm^{-1} between peaks and a minimum peak height of 50 counts, the peaks for fitting may be identified. Good agreement is found with literature values, for example those presented by Salvaggio et al.[24] and Yagoubi et al.[25] These peaks are presented in full in Table A1, along with peak assignment based on the mentioned literature for the carbonyl region.

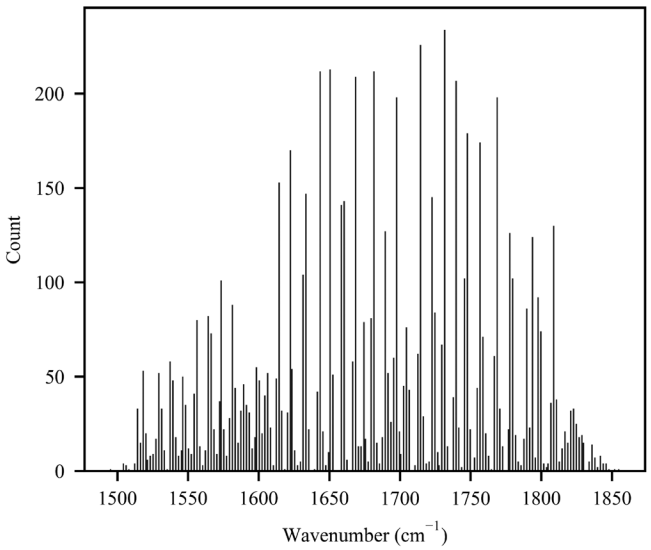

FIGURE 2 Attenuated total reflectance Fourier-transform infrared spectroscopy (ATR-FTIR) peak positions between 1500 and 1850 cm^{-1}.

The carbonyl index of a specimen may be calculated in a variety of ways, typically based on standardizing the carbonyl peak area or maximum height against that of a reference peak. The present state-of-the-art technique, by Almond et al.[27] makes use of the ratio of areas between 1650 and 1850 cm^{-1} (carbonyl) and 1420 to 1500 cm^{-1} (reference, methylene scissoring peak) after baseline correction. Knowing, however, that the peaks in the region of 1790 to 1810 cm^{-1} are associated with calcium carbonate, and would therefore skew results if not compensated for, this method cannot be used directly.

At first, it may be tempting to make use of curve fitting in the hopes of determining all of the constituent peaks directly, as is sometimes claimed in the literature.[24,25] However, given the large number of peaks in the carbonyl region (Figure 3A,B) and the (potentially) four degrees of freedom per peak (position, shape, height and width), overfitting is a distinct risk—particularly at the typical 4 cm^{-1} resolution for this analysis. This continues to be true in the event that the peak centres are fixed to those identified using global peak finding and the peaks are fixed to a Gaussian profile (owing to the

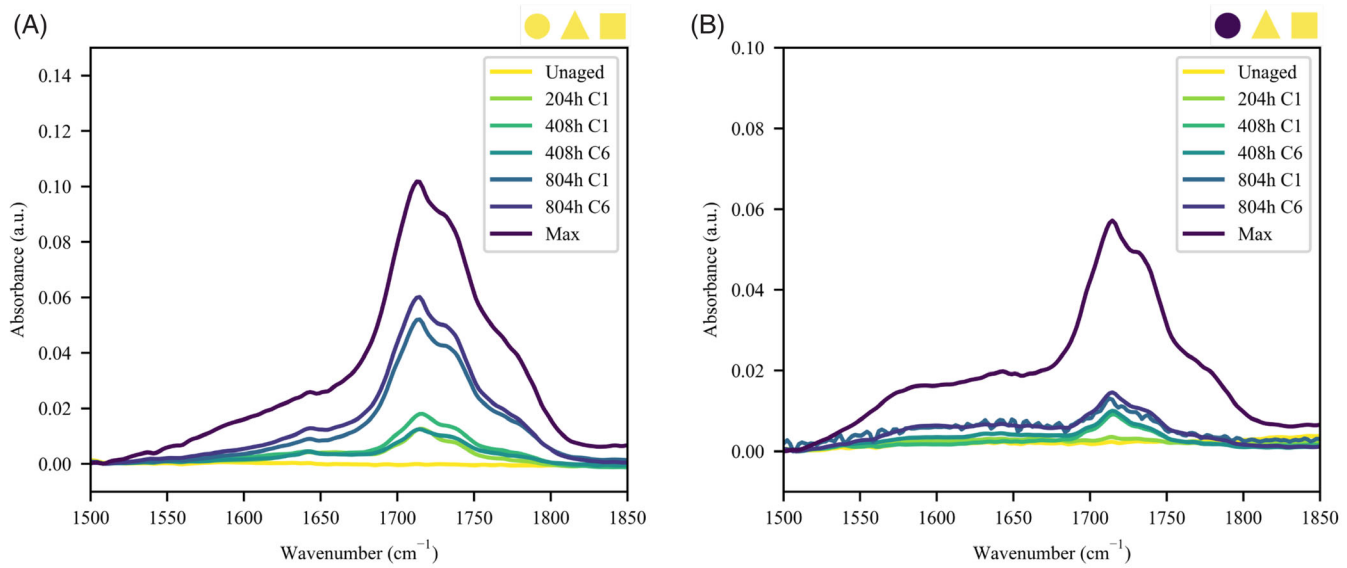

FIGURE 3 Attenuated total reflectance Fourier-transform infrared spectroscopy (ATR-FTIR) profile between 1500 and 1850 cm^{-1} for (A) the front surfaces of REF specimens of the virgin material and (B) the 3.6CB/0CC/0S material.

solid-state material under investigation here). A straightforward check for this exists, however, in that γ-ketoacids possess two groups with peaks in the carbonyl region (a keto group (1698 cm^{-1}) and an acid group (1707 cm^{-1})), where the extinction coefficients of the groups are known—allowing for a ratio of peak heights to be estimated. If the ratio of the fitted peaks is far from the desired ratio, with the acid group having an intensity of 2.1 to 2.4 that of the keto group,[24,26] it is likely that the fit is in error.

Extensive curve fitting was trialed for this work, but it proved impossible to find stable fits that were internally consistent with the progression of degradation while maintaining the γ-ketoacid ratio. As a result, these fits are compressed to yield an estimate of the isolated carbonyl region, free of the double-bond and calcium carbonate peaks, where a high quality of fit was achieved. Thereby, a calcium-carbonate-free carbonyl area can be estimated, with the carbonyl index here based on the ratio of the area of the (carbonyl-stretching) peaks between 1680 and 1790 cm^{-1} and that of CH_2 and CH_3 stretching peaks (between 2680 and 3020 cm^{-1}).

The result of this is illustrated for the complete dataset in Figure 4, and as a function of formulation in Figure 5A,B, for the highest aging level. Here, it can be seen most clearly that 0CC/0S formulations exhibit much more significant front-surface oxidation than the remaining formulations—reiterated in Figure 6. The opacifying effect of the CB can clearly be seen in Figure 5B, where the back-surface oxidation of the 3.6CB/0CC/0S material is much more in line with the stabilized 0CC materials, while the 0CB/0CC/0S material still shows more

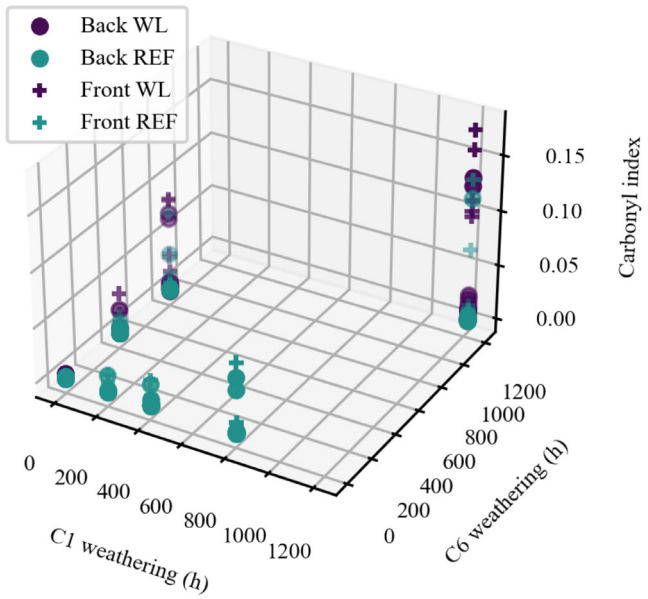

FIGURE 4 Carbonyl index as a function of weathering time and type for all materials.

significant oxidation than that seen in other materials. Also clear is the effectivity of the stabilizer package, across the full range of formulations. CB, on the other hand, appears to exhibit more complex behavior—with differing slopes with increasing CC for the front and back surfaces of specimens.

If Figure 5 is compared with Figure A1A,B, it is clear that the omission of the CC peaks from the carbonyl index have aided the comparability of the materials, by removing the positive slope associated with increasing

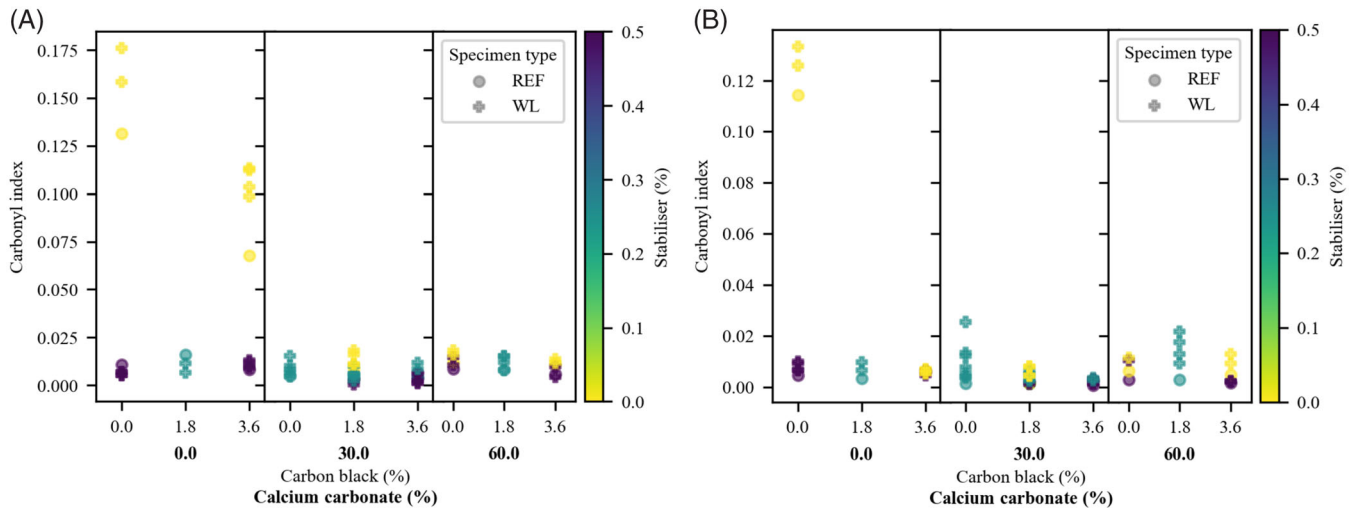

FIGURE 5 (A) Front and (B) back carbonyl indexes as a function of formulation and specimen type for the materials exposed to the maximum weathering level.

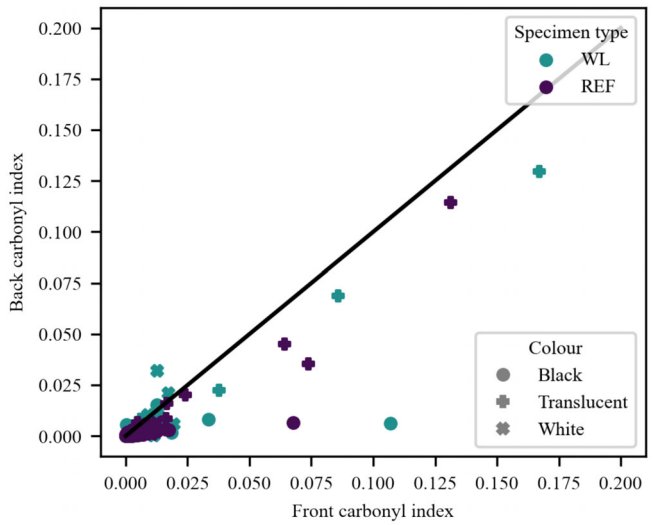

FIGURE 6 Comparison of front and back carbonyl indexes for all specimens and aging levels.

CC in Figure 5A,B. If, further, Figure 5 is compared to Figure A1C, D (which represents the results obtained using the Almond et al.[17] technique, adapted to omit the carbonate peaks), a strong similarity may be observed. The combined-fitted-peak method is preferred, as it may better tolerate complexities stemming from increased levels of non-carbonyl species.

From Figure 6, it would appear that the CI on the fronts of the specimens is consistently higher than that on the backs of the specimens. This could be confirmed through the use of a t-test, based on the mean CI of each combination of formulation, specimen type and aging level, with a p-value of 1.35×10^{-6}. Here, the unaged specimens were omitted from consideration. As indicated by a Pearson correlation coefficient of 0.878, a strong and positive correlation exists between the front and back CIs, albeit with a substantial variation in slope as a function of formulation. It is interesting to note the high front CI contrasted by the low back CI of some of the black specimens, suggesting that the fronts of some of these materials are sensitized to degradation. Owing to the thinness of these specimens, it is unlikely to be the effect of temperature alone—but may result from the combined effect of temperature and radiation, as well as the degradation of the SEBS introduced with the CB.

Further, based on Figure 6, it would appear as though the WL specimens have higher CIs than the REF specimens. This, again, could be confirmed with a t-test, based on the mean CI for each combination of formulation and aging level, with a p-value of 0.01 for the fronts of the specimens and a p-value of 3.2×10^{-4} for the backs of the specimens. This is particularly interesting, when considering that the p-value of the same test, but limited to the unaged specimens, is 0.51—suggesting that the WL and REF specimens experience differing rates of oxidation to allow for the statistically significant difference between then despite the insignificant initial difference.

Using these data, it was not possible to definitively show that C6 weathering results in more aggressive oxidation than that caused by C1 weathering, with p-values (also by t-tests on the means of material and aging time combinations of REF specimens) of 0.29 and 0.44 for the fronts and backs of the specimens.

In terms of the effects of the additives and time, outlined in Table 3 based on a model of the form given in Equation (2), it is comforting to see that CI increases with

TABLE 3 Interactive effects of weathering time with the formulational variables and their interactions on the measured carbonyl and double-bond indexes of specimens.

Measures	Side	Type	t	t:CC	t:CB	t:S	t:CC:CB	t:CC:S	t:CB:S	$t:CC^2$	$t:CB^2$	$t:S^2$
Carbonyl index	Front	REF	↗	↘	↘	↘	→	↗	→	→	→	→
Carbonyl index	Back	REF	↗	↘	↘	↘	→	→	→	→	→	→
Carbonyl index	Front	WL	↗	↓	↘	↘	→	↗	→	↗	→	→
Carbonyl index	Back	WL	↗	↘	↘	↘	→	→	↗	↗	•	•
Double-bond index	Front	REF	↗	N/A	↘	↘	N/A	N/A	•	N/A	↗	↗
Double-bond index	Back	REF	↗	N/A	↘	↘	N/A	N/A	↗	N/A	↗	↗
Double-bond index	Front	WL	↗	N/A	↘	↓	N/A	N/A	↘	N/A	↑	↗
Double-bond index	Back	WL	↗	N/A	↓	↓	N/A	N/A	↗	N/A	↗	↗

time—increasing more sharply for the fronts of the specimens than for the backs. Similarly, the effects of the additives are, generally, stronger on the fronts of the specimens. It is notable that all of the effects share direction across the sides and types of specimens, except for the $t:CB^2$ and $t:S^2$ terms that are not significant and one instance of a CB:S term. The strong negative primary effects of the additives show their effectivity in mitigating oxidative degradation, through blocking (CB and CC) and chemical means (S). The remaining effects are positive, albeit insufficiently so to undo the gains through the primary effects. The squared terms indicate the diminishing effects of the additives with increasing loading, while the interactive terms indicate reductions in effectivity for mixed systems. Overall, this would suggest that lower levels of additives are generally very effective, with reduced gains found by increasing loading or the introductions of more additives. The strongest of the interactive effects is that of CC:S, which is expected to reflect this, given the very strong primary effects of CC and S.

$$\widehat{y} = t\left(\widehat{\beta}_0 + \sum_{i=1}^{p}\widehat{\beta}_i x_i + \sum_{i=1}^{p}\sum_{j=i}^{p}\widehat{\beta}_{ij}x_{ij}\right) \quad (2)$$

A double-bond index (DBI) may be constructed in a similar vein to the carbonyl index, here focusing on peaks between 1500 and 1680 cm^{-1}, to account for acyclic and aromatic unsaturations. As a result of overlap with the large and broad CC peak centered around 1400 cm^{-1} conflicting with the fitting algorithm, the CC-containing materials are omitted from this discussion. The broad range is based on inspection of the FTIR profiles of the relevant materials, such as in Figure 3A,B. These profiles appear to exhibit aromatic C—C bonds and C═C bonds. The aromatic C—C bonds, with a primary peak around 1580 cm^{-1}[27,28] are present throughout, particularly with increased aging, but are much more prominent in the materials containing CB. At the same time, the terminal C═C bonds exhibit a broader peak around 1650 cm^{-1}[29,30] in the CB-containing materials than in those without, suggesting greater diversity in the character of these bonds. It is possible that additional groups are present in this region, particularly in the materials with CB, but insufficient resolution is available to distinguish these moieties.

Seen in Figure 7A, is the DBI at the maximum aging level. T-tests may be used to confirm the suspected higher DBI for WL specimens than for REF specimens (p-values of 0.029 and 0.048 for the fronts and backs of the specimens), but no significant systematic differences were found between the DBIs of the fronts and back of the specimens (p-values of 0.18 to 0.37 for the WL and REF specimens). Notable, however, is the behavior of the 3.6CB/0CC/0S WL specimens, presented in Figure 7B, where an initial slow growth in DBI experiences explosive growth on the fronts of the specimens between the 804 h and maximum weathering steps—exhibiting a higher DBI than even that of the virgin material (which exhibits a much more linear increase in DBI). This growth is not matched by the backs of the specimens, indicating that a critical level of degradation was reached, after which a 'runaway' reaction takes over in these specific specimens. This lends further weight to the idea that the SEBS masterbatch of the CB is subject to degradation by exposure to UV light but that the CB is effective at stopping the propagation of the UV radiation through the sample.

Based on analysis of the complete data with a model of the form given in Equation (2) (but with the CC terms omitted), with the effects given in Table 3, consistent effects can be seen. Again, the DBI increases

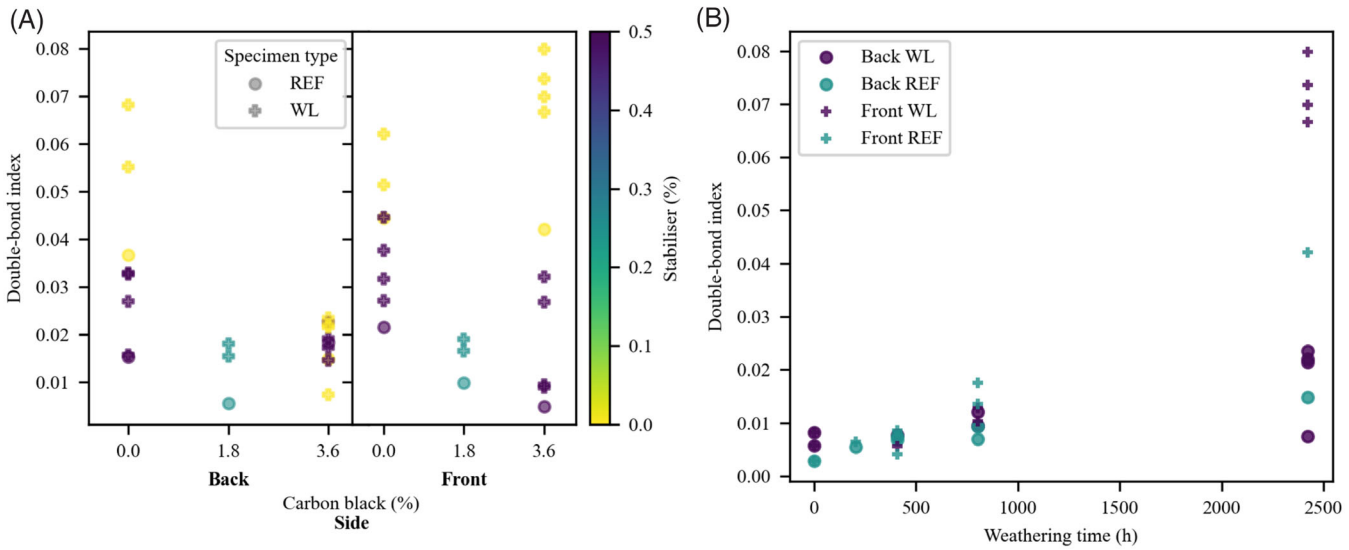

FIGURE 7 (A) Comparison of front and back double-bond indexes as a function of formulation and specimen type at the maximum aging level. (B) Comparison of front and back double-bond indexes as a function of specimen type and aging level for the 3.6CB/0CC/0S material.

with aging time, and this is strongly counteracted by CB and S. The effects of these, though, diminish with increasing loading. The back sides of the specimens exhibit antagonism between CB and S, while the front of the WL specimens exhibits a synergy between these additives.

Finally, a "carbonate index" can be used to investigate the possibility of CC being leached from the specimens as a result of the moisture cycles that they are exposed to. This index is taken as the ratio of the sum of the areas of the peaks between 1790 and 1810 cm^{-1}[31–33] to that of the typical reference peaks. The zero values are omitted here, again as a result of the fitting function used. The results of this are presented in Figure 8, where it can be seen that the reduction in carbonate index is at first rapid, slowing as it approaches the asymptote at zero. Curiously, there appears to be much increased unexplained variance in the WL specimens, in addition to generally higher levels. The higher levels for the WL specimens may be confirmed for the fronts of the specimens, based on a p-value of 1.5×10^{-4}, but the findings for the backs of the specimens are insignificant, based on a p-value of 0.33 across aging levels present for both specimen types. No significant difference could be found in the means of the front and back sides of the specimens, with p-values of 0.89 (REF) and 0.52 (WL).

3.2 | Tensile properties

The effects of weathering varied dramatically between materials and measures, as exhibited, for example, in Figure 9. These are presented as Property Retention Indexes,[34] based on the measures on unaged materials, and denoted by the "adjusted" prefix to a measure. The stress–strain curves for the specimens are presented between Figures A2 and A5.

First, it was sought to determine if the type of weathering had a significant effect on the mechanical performance of the specimens. Thereby, t-tests were performed on the mean properties of REF specimens of each formulation at relevant aging levels. Accordingly, this was performed for the 4 parameters of interest: Young's modulus (p-value of 0.034, C1 greater than C6), yield strength (p-value of 0.735), elongation at yield (p-value of 0.35) and elongation at break (p-value of 0.67). This suggests that the stiffness of the material is more susceptible to the type of aging applied than are the other parameters. What is more, if another t-test is performed on the difference in mean YM between C1 and C6 for the 408 and 804 h aging levels, it may be found that the difference is significantly (p-value of 0.030) more pronounced at the 408 h level. This appears to be particularly present in the specimens without CB, suggesting that the early changes experienced by these specimens vary as a result of radiation intensity, but that this difference is lessened with increasing aging.

Next, the different ways of incorporating the carbonyl index are compared—based on Equation (3) and presented in Figure 10A,B. Compared were four options: (1) only front carbonyl index (FCI), (2) only back carbonyl index (BCI), (3) mean of front and back carbonyl indexes (MCI), and (4) front and back carbonyl indexes (resulting in model size being doubled). The Akaike Information Criterion (AIC, lower better) and adjusted R^2 (higher better) penalize model complexity, in an effort

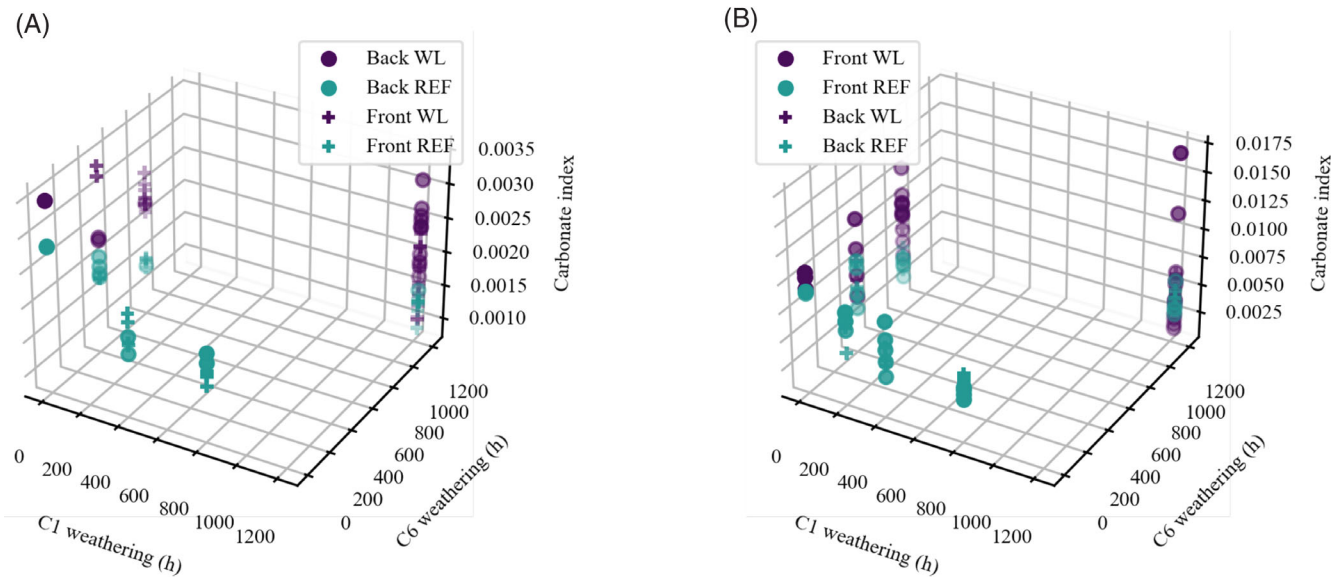

FIGURE 8 Comparison of front and back carbonate indexes as a function of aging time and specimen type for the (A) 30CC materials and (B) 60CC materials.

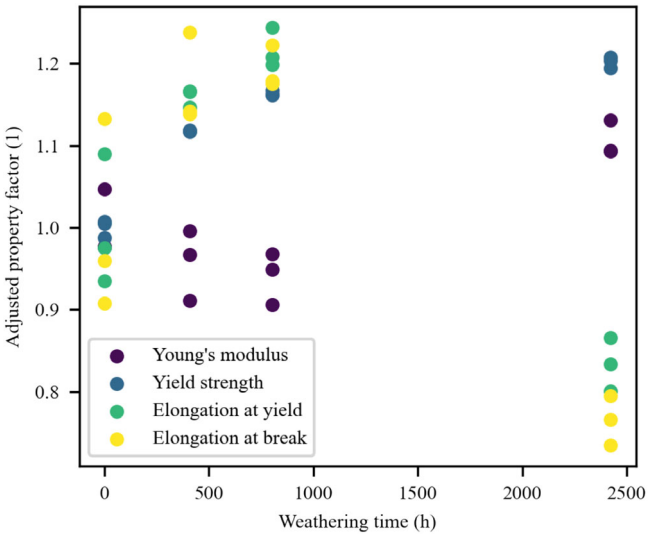

FIGURE 9 Property progression as a function of weathering time for WL specimens of the 0CB/30CC/0.25S material.

to enable fairer comparison. It must be kept in mind, however, that AIC is affected by the number of data points—with more points offering a better score. Nonetheless, the combined model offered the best fit. Somewhat surprisingly, the MCI model was, on average, outperformed by the FCI model, while the BCI model was consistently the worst. This suggests that the uneven propagation of degradation through specimens of the different materials has a noticeable effect on the tensile properties of the specimens. Moving forward, the combined model will be used as it offers the best fit.

$$\widehat{y} = CI\left(\widehat{\beta}_0 + \sum_{i=1}^{p}\widehat{\beta}_i x_i + \sum_{i=1}^{p}\sum_{j=i}^{p}\widehat{\beta}_{ij}x_{ij}\right) \tag{3}$$

Finally, the predictive strength of different ways of accounting for weathering was compared. The first method would directly use the amount of time exposed to weathering, while the alternative would use the carbonyl index as a proxy for the degree of degradation and would additionally enable the study of the interactive effect of carbonyl index and formulation on the mechanical properties of the system. Summaries of the trial fits are presented in Figure 10C,D, for models of the forms given in Equations (2) and (3). For the sake of simplicity and as a result of the insignificant effect of aging type, all weathering time models make no distinction between C1 and C6 weathering. Based on this, it is clear that carbonyl index is a far stronger indication of the degree of degradation than the amount of weathering alone. It is also clear that the unexplained variance of the weld-line specimens is generally much lower than that of the reference specimens, as a result of the weld-line v-notches serving as failure initiation points. The raw data are presented as a function of weathering type and time, for simplicity and a more intuitive understanding of the performance of the materials.

3.3 | Young's modulus

The adjusted Young's moduli (aYM) of the materials, Figure 11, show mixed effects, with some materials

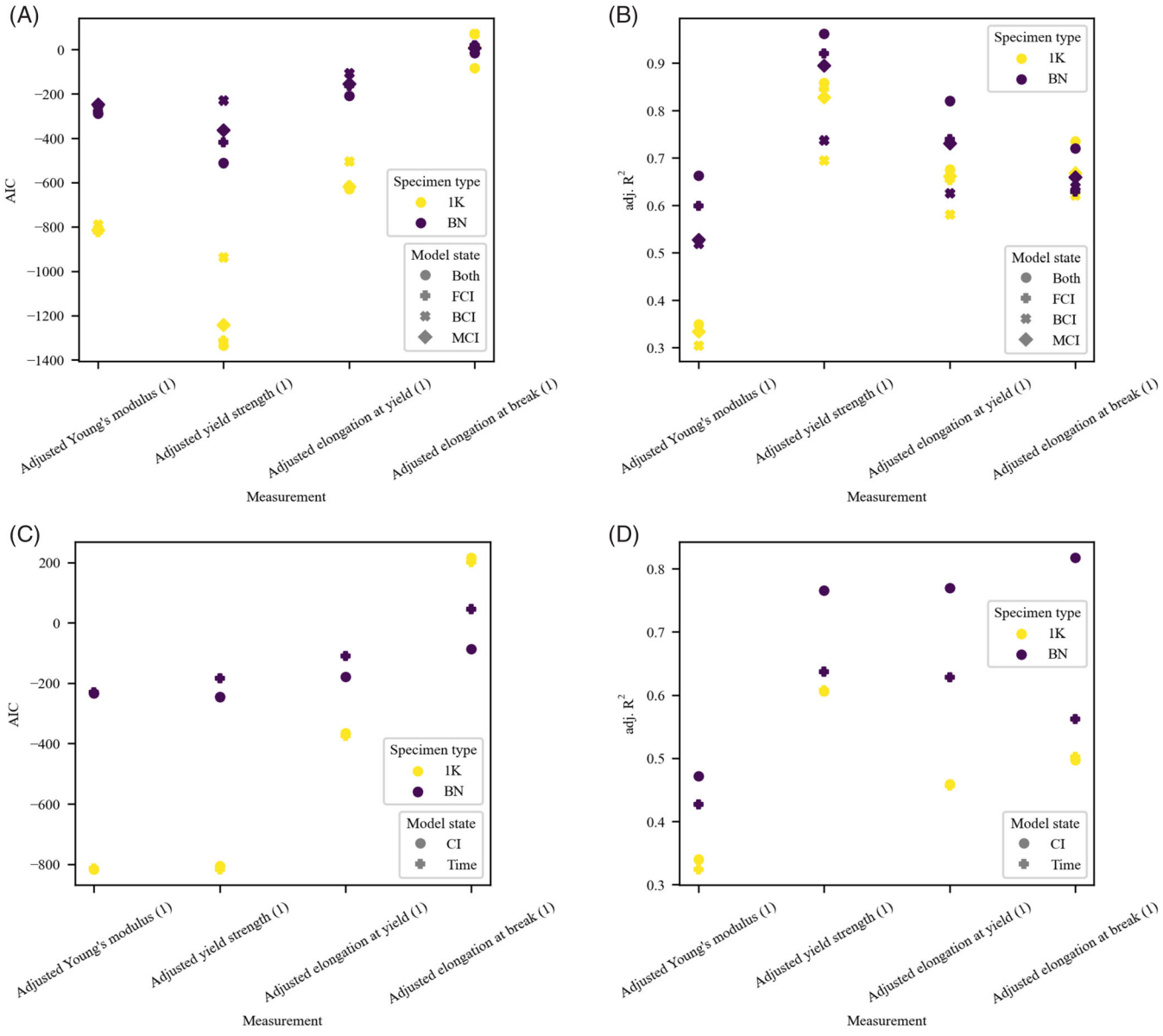

FIGURE 10 Quality of fit metrics: (A) AIC for different CI models; (B) R^2 for different CI models; (C) AIC for comparison of CI and weathering-time models; and (D) R^2 for comparison of CI and weathering-time models.

exhibiting a moderate increase (up to about 30%) in stiffness with weathering, while others see moderate to strong decreases (40% to 60% for the virgin material). Nonetheless, the results appear to be subject to fairly high variance—particularly in the case of the reference specimens—which is confirmed through the weak quality-of-fit metrics found during statistical analysis. The addition of CB, CC or S seems to lessen the degree of property loss with aging as compared to the virgin material, although, broadly, it would appear that an increase in CB loading results in a more negative tendency. What is more, some materials exhibit peaks—or even unabated increases—in their stiffness at varying levels of aging, while others exhibit monotonic decreases. The specific statistical effects are discussed in the dedicated subsection.

3.4 | Yield strength and elongation at yield

The adjusted yield strengths (aYS), Figure 12A,B, and adjusted elongation at yield (aEaY), Figure 12C,D, of the materials may be dissected into two sections: the materials that experienced severe aging (0CB/0CC/0S and 0CB/60CC/0S) and those not as affected by weathering. In the materials affected by severe aging, the typical degradation of properties with increasing aging may be seen,

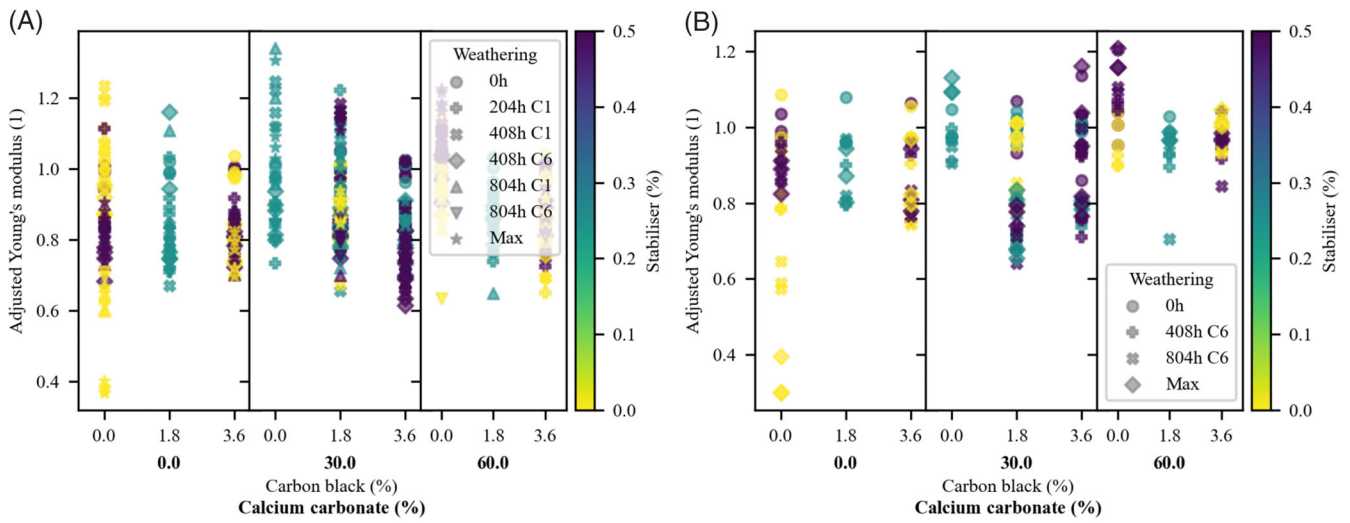

FIGURE 11 Comparison of adjusted Young's modulus as a function of aging time and formulation for (A) REF and (B) WL specimens.

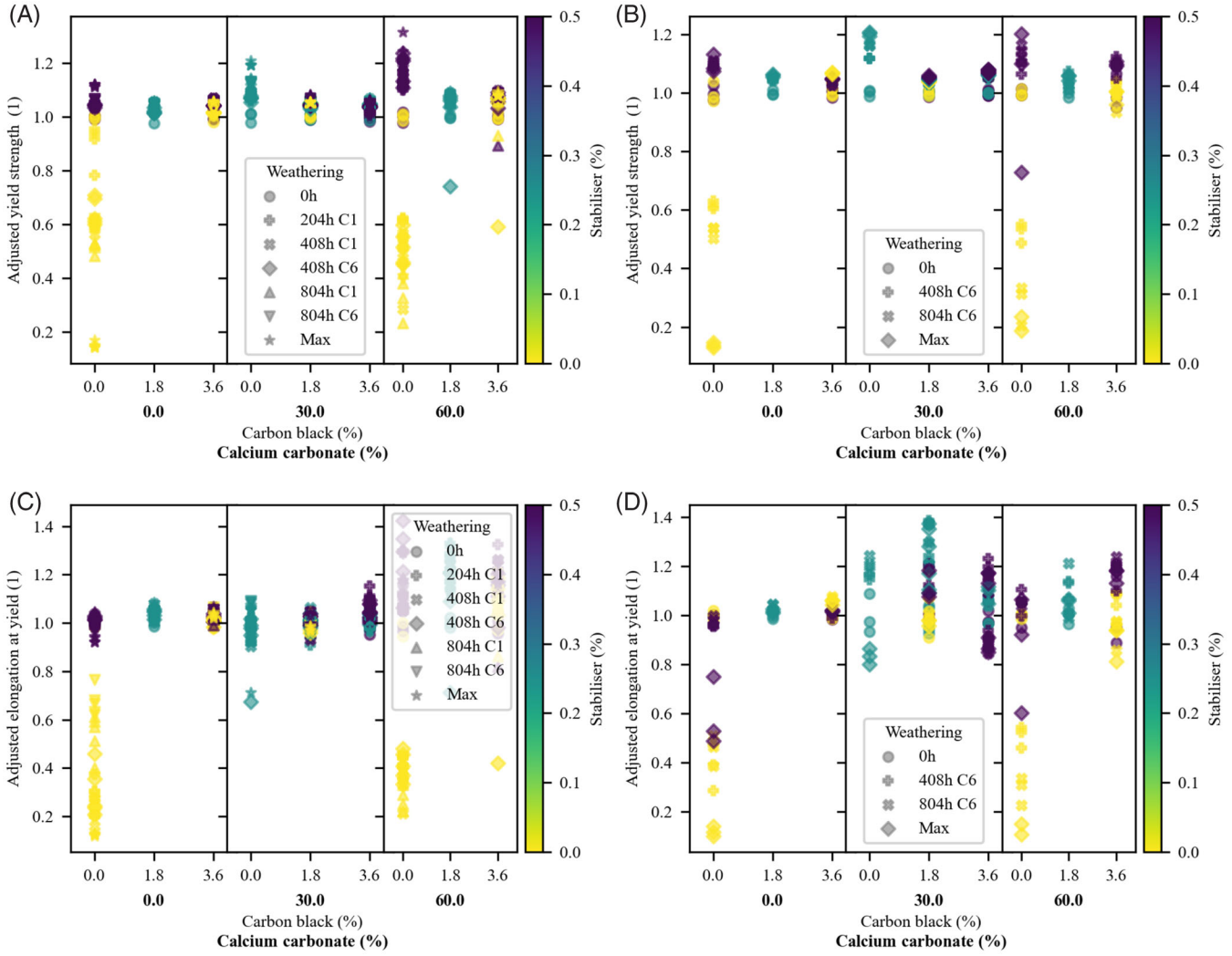

FIGURE 12 Comparison of adjusted yield strength as a function of aging time and formulation for (A) REF and (B) WL specimens. Comparison of adjusted elongation at yield as a function of aging time and formulation for (C) REF and (D) WL specimens.

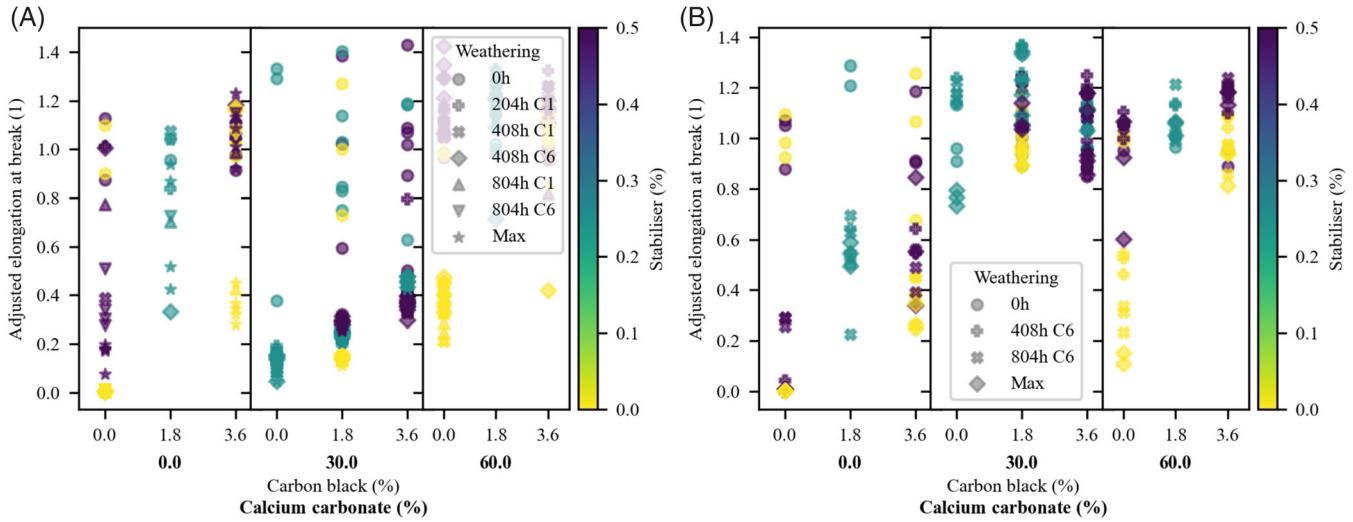

FIGURE 13 Comparison of adjusted elongation at break as a function of aging time and formulation for (A) REF and (B) WL specimens.

while the opposite—albeit much less severe—can be seen in the more resilient materials. It is clear that additive effects are present in this latter regime, and worth noting that some of the specimens—such as the 0CB/0CC/0.5S and 0CB/30CC/0.25S WL specimens subject to the maximum aging level—are starting to bridge the gap between the classifications (particularly in terms of aEaY).

3.5 | Elongation at break

The adjusted elongation at break (aEaB), Figure 13, of the materials exhibit the largest shifts in the mechanical properties of the materials, albeit coupled to the largest variance (particularly in the case of the REF specimens). From these data, a stark shift in EaB can be seen in the 30CC REF specimens, with increasing aging, consistent with the observed shift to brittle fracture. These samples exhibit the most consistent degradation of properties with aging time, with some exceptions where the specimens exhibit peaks followed by reductions in EaB.

3.6 | Parameter effects

T-tests were performed to determine whether any systematic differences in the adjusted mechanical properties existed between the WL and REF specimens, for all formulations and shared aging levels. The only significant difference was found for aEaB, with the WL specimens outperforming the REF specimens with a p-value of 1.2×10^{-3}. This is the result of the transition to brittle failure experienced by the 30CC REF specimens with aging, compared to the equivalent WL specimens that already fail in a brittle fashion without aging. aYM, aYS and aEaY showed insignificant effects, with p-values of 0.51, 0.21 and 0.35.

Taking an overall view of the parameter effects in terms of time, as summarized in Table 4, it is clear that the parameters tend to have consistent effects across measures. Aging time is the first of these, with a consistent negative impact (as may be expected). Also expected are the generally positive effects of the addition of stabilizer (shown through the t:S term), albeit with these effects approaching an asymptote with increasing loading (the broadly negative $t:S^2$ term). These types of effects are also seen for CB and CC, albeit with a couple of exceptions. The positive $t:CB^2$ term is clearly reflected in the aYM data for the WL specimens. The negative t:CC and positive $t:CC^2$ terms for the aEaB data for REF specimens point towards the strong curvature as a function of CC on the aEaB of those specimens—this is more of a secondary effect of the switch to brittle failure present in the unaged 60CC specimens, while the 30CC specimens transition towards this with increasing degradation. This is motivated by the strong performance of the 30CC materials in aEaB for WL specimens, where brittle failure is also present from the unaged specimens.

General trends can also be seen across the interactive effects with time, with dominant antagonistic behavior for CC:CB and CB:S countered by primarily (albeit weak) synergism for CC:S.

If the 0CB/0CC/0S and 0CB/60CC/0S cases and suspected outliers are omitted from the statistical analyses for aYS, a clearer understanding of the subtler remaining effects may be gained. Seen in Table 4, increasing CB

TABLE 4 Interactive effects of weathering time with the formulational variables and their interactions on the adjusted mechanical properties of specimens.

Measure	Type	t	t:CC	t:CB	t:S	t:CC:CB	t:CC:S	t:CB:S	t : CC^2	t : CB^2	t : S^2
aYM	REF	→	↗	●	→	→	●	→	→	●	●
aYM	WL	→	→	●	→	→	→	→	●	→	●
aYS	REF	↘	→	↗	↗	●	→	↘	→	→	→
aYS	WL	↘	→	↗	↗	●	●	↗	→	●	→
aEaY	REF	↘	●	↗	↗	●	→	↘	●	→	→
aEaY	WL	↘	→	↗	↗	●	→	→	→	→	→
aEaB	REF	↘	↘	↗	↗	→	–	→	↑	●	→
aEaB	WL	↘	↗	↗	↗	●	→	●	↘	→	→
aYS*	REF	→	→	→	●	→	●	●	●	→	●
aYS*	WL	→	●	→	→	●	→	→	●	→	●

TABLE 5 Interactive effects of CI with formulational parameters and interactions on the adjusted mechanical properties of specimens. A front/back format is used to present the data in a more compact form.

Measure	Type	CI	CI:CC	CI:CB	CI:S	CI:CC:CB	CI:CC:S	CI:CB:S	CI : CC^2	CI : CB^2	CI : S^2
aYM	REF	● ●	→ ●	→ →	● ●	→ ●	→ ●	→ ●	→ ●	→ →	● ●
aYM	WL	● ●	● ●	● ●	→ →	● ●	● ●	● ●	● ●	● ●	→ →
aYS	REF	→ ●	→ →	– ●	→ –	→ →	→ →	→ ●	→ →	● ●	● ●
aYS	WL	→ →	● ●	→ →	● ●	→ →	● →	→ →	● →	→ ●	→ →
aEaY	REF	● →	● ↘	● ●	● ●	→ →	→ →	→ ●	● →	● –	● –
aEaY	WL	→ →	● ●	→ ●	→ →	● ●	● →	→ →	● →	● ●	● ●
aEaB	REF	→ →	↘ ↓	→ ●	● ↗	→ ↘	● ↗	● ●	↗ ↑	→ ↗	● ↘
aEaB	WL	→ →	● ●	● ●	● ↘	● →	● →	● →	● ↘	– ●	● ●

results in diminishing positive effects in REF and WL specimens. In these more stable materials, an improvement in aYS is seen with aging time. Beyond that, a weakly positive correlation exists with CC for the REF specimens, set against an antagonism between CC and CB. Curiously, the WL specimens do not exhibit these effects, but rather a weakly negative effect for S and synergisms between CC:S and CB:S.

If, now, considering the combined effects of carbonyl index and formulation, as presented in Table 5, much less homogenous behavior is found, albeit, typically, with increased descriptive power over the mechanical performance as mentioned at the start of section. From these results, it is clear that the effects are mild throughout, with the most sensitive measure to aging being aEaB. It is interesting to note that the effects of parameters with FCI and BCI are rarely in agreement. As shown in Figure 6 above, BCI generally trails FCI, meaning that the effect of the BCI-related terms must be greater than those of the FCI-related terms to have the same impact at a given aging level.

The primary effects of FCI are consistently more negative than those of BCI, which are, surprisingly, frequently positive. This bears more discussion, as it would

seem natural that BCI would have a more negative impact than FCI, as a result of representing the progression of degradation through a specimen. This may be a result of covariance between these variables, with BCI trailing FCI in an almost autoregressive fashion—resulting in the positive terms for BCI acting to induce curvature as a function of time.

The synergy of CC:S is again present, and fairly consistent. The BCI:CB:S terms also tend to be positive, contrasted by negative terms for FCI:CB:S.

The strong negative terms for CC in the aEaB measure of the REF specimens, offset by the strong positive terms for CC^2, are indicative of a strong negative effect lessening with increasing CC loading. These are the strongest terms in the studied system, while the remainder are fairly mild by comparison. Keeping in mind the reference point of unaged virgin material, extended to aged virgin material through the CI terms, positive terms refer to the material performing proportionally better at a given level of CI than the virgin material.

As a result of the uneven findings, attributing behavior to specific processes may be haphazard at best. However, it is clear that the additives not only affect the propagation of degradation through the specimens, but also the mechanical response of a degraded specimen and, likely, the degradation mechanisms themselves.

4 | DISCUSSION

The carbonyl index growth profiles of the materials here studied match those seen elsewhere, for example in Pěna et al.'s[9] studies on additive synergism in combating the photodegradation of LDPE, with an apparent two-step process. The carbonyl index grows exponentially from unaged, only to be slowed in a very sharp inflection point, followed by a second phase of accelerating growth.

Based on the FTIR data presented, it is clear that the autocatalytic degradation of the materials is complex and not limited only to the development of carbonyl groups, but also that of double bonds. The groups formed appear to be strongly influenced by formulation, clearly illustrated, for example, by the comparison of the double-bond regions of Figure 3A,B—where the material containing CB exhibits not only a much higher proportional growth in double-bond character, but also that the double bonds are of different types to those developed in the virgin material. The enhanced rate of degradation with an increase in the number of double bonds is in agreement with the findings of Gryn'ova et al.[2] in terms of the auto-oxidative pathway becoming more energetically favorable as a result of the presence of these and oxidative defects. What is more, the development of peaks corresponding to aromatic and conjugated C—C bonds in the 1500 to 1600 cm^{-1} region suggest the presence of significant change to the character of the HDPE chains beyond scission/long-chain branching and the terminal C═C bonds seen in the less-aged materials. This is an important consideration for future work, particularly given that the carbonyl index is frequently reported alone.

The leaching of calcium carbonate, as suggested by Figure 8, is to be expected—despite the low solubility of calcium carbonate, lessened further by its stearic-acid coating—given the duration of the specimens' exposure to moisture. It is likely that this leaching is limited to the surface of the specimens, given the similarity in stiffness across aging levels and the limited penetration depth of ATR-FTIR techniques. The leaching may, however, leave pores in the surface. This would need to be closely monitored, particularly as the composites consist of food-safe components and materials of this type may be used in food-contact applications.

The differences between the fronts and backs of the specimens, in terms of CI, are to be expected. Naturally, radiation—and, thereby, degradation—propagates much more easily through the translucent specimens, pointing towards the blocking effects of CB and CC. Similarly, the pure-additive effect of S can be clearly seen by comparing the 0CB/0CC/0S and 0CB/0CC/0.5S materials. The insignificant difference seen in DBI between the fronts and backs of the specimens is not an indication of a lack of difference, but rather is symptomatic of the lower signal-to-noise ratio of these measurements. The authors believe that, with a larger data set and increased aging, this difference will become significant as a result of the underlying mechanisms at play and the strong influence that radiation has on this degradation. The lack of significant difference between C1 and C6 aging would suggest that radiation is not significantly a limiting variable in the degradation of these materials, but further work would be needed to confirm that.

Less expected, are the findings of increased CI and DBI for the WL specimens compared to those of the REF specimens. This, in theory, could stem from differences in processing-induced degradation, but this is unlikely given the insignificant differences in the indexes for these specimens before aging was performed. Rather, the authors believe that these differences stem from differences in the processing-induced morphology of the specimens, compounded with the observational effects of ATR-FTIR. In particular, the WL specimens are expected to possess thinner (highly crystalline) skin layers as a result of their shorter flow paths, with these offering less protection to the less crystalline cores of the specimens than that offered by the thicker skin layers of the REF

specimens. As it is known that auto-oxidative degradation primarily occurs in the amorphous regions of HDPE,[35] it would follow that the specimens with larger highly crystalline barriers to degradation would be more stable. At the same time, it is known that ATR-FTIR has a shallow penetration depth, which may amplify the perceived difference between the specimens as a result of the different thicknesses of the skin layers.

Clearly, the additives have primary stabilizing effects, in reducing the carbonyl and double-bond indexes. This is to be expected, as all three compounds are known to improve the weathering resistance of formulations in which they are used. Less discussed is the diminishing effect of the additives with increasing loading, suggesting that their effectivity decreases with increasing loading. The interactions of the additives are also negative, suggesting that similar reductions in effectivity are seen through the combination of additives. This, likely, points towards overlap in their effects on the limited amount of aging performed, where CC and CB tend to minimize light passing through the specimens and CB (through acting as a light barrier even at low loadings) and S have stabilizing roles. Chemical antagonism, for example through the adsorption of S onto CB and CC,[1,9] may also play a role. In the case of the double-bond index, more complex effects may be considered, where, potentially, the synergy seen for CB and S on the front surface may be the result of the stabilizing effect of S on the SEBS accompanying the CB, while the antagonism on the back surface may be ascribed to the overlap in roles of the additives.

Despite all of these changes, though, the stabilized materials maintain their usable mechanical properties well—frequently improving with aging up to the levels here investigated. It is important to consider that while improvements in properties are better than reductions in those properties, the goal of stabilization is to keep the material near its initial state. It is likely that, with increased aging, the positive changes will be reversed,[7] and the materials that have exhibited the fastest positive change would also be subject to the most rapid degradation of their properties. The first traces of this can be seen, with clear examples of the 0CB/0CC/0.5S and 0CB/30CC/0.25S WL specimens in terms of their EaY. The additive effects discussed in the prior paragraph are, broadly, mirrored in the retention of mechanical properties, with positive primary effects and negative squared and interactive effects. A notable exception exists, however, in the CC:S interaction that is broadly positive. This interaction has been noted in prior works on these materials,[15,19] and is expected to be the result of the stabilizing effects of S on the specimens highly filled with CC that are much more prone to processing degradation as a result of their dramatically increased viscosity.

The increase in the tensile strength of HDPE with aging has been noted elsewhere, typically in highly stabilized materials and cases with thicker cross-sections.[7]

Little significant difference in the development of mechanical performance with aging was found between WL and REF specimens, serving as something of a surprise given the higher levels of degradation products detected in the WL specimens. This suggests that, with a much larger sample size, more can be learned about the differences in degradation as a function of specimen type, but also that these differences are relatively small. The significant difference in EaB is the result of a shift to brittle failure in the 30CC REF specimens with aging, discussed later in this section.

The 0CB/0CC/0S and 0CB/60CC/0S materials stand somewhat alone in terms of the changes in their usable mechanical behavior with increasing weathering, particularly in terms of YS and EaY. These materials exhibit dramatic degradation in these properties with increasing weathering, much more, in line with what is typically reported in the literature.[7,36,37] These materials may be considered to be unstabilised, in the 0CB/60CC/0S case the blocking effects of the CC are offset by more significant processing-induced degradation.

When the mechanical properties are viewed as a function of formulation and carbonyl index, much more complicated results are obtained, and the model fit is improved—clearly illustrating the correlation between the changes in the chemistry of the materials and those in the mechanical properties. These point towards the complex mechanical effects of the chemical changes brought about by degradation not only in the matrix but also in the additives. The effects of the propagation of degradation can also clearly be seen through the effects of FCI and BCI frequently having reversed directions. Rightly, this would suggest that specimens where the degradation is localized near the front surface behave quite differently, to those where degradation propagates through the specimens to a greater degree, notable in that the absolute values of the BCI effects tend to be greater than those of the FCI effects. A clear exception to the differing directions of FCI and BCI effects are those of CC:S, with these additives exhibiting synergisms in this context as well.

The changes in the resistance of the amorphous regions to extension primarily resulting in the bulk material stiffness reported as YM are, broadly, sensitive to chain scission, long-chain branching, cross-linking and the introduction of carbonyl groups and double bonds. These effects, largely, stem from changes to the mobility of chains in the amorphous region where, for example, chain scission allows for increased freedom of motion for the free ends in the amorphous region, and an increase

in the number of these ends, but with a decrease in the size of the region through increased crystallinity. Given the predominantly negative trend with increasing aging, it is likely that chain scission is the dominant effect in this context.

YS serves as an indication of the resistance of the material to lamellar slip, allowing a probe into the changes affecting the crystalline regions of the matrix. In the materials containing CB or S, an increased resistance to lamellar slip can thus be seen. This, likely, is the result of increased crystallinity stemming from chain scission during the degradation of the specimens, as has been reported elsewhere for HDPE.[38]

The competing effects of changing resistances to amorphous extension and lamellar slip can be seen in EaY, where the materials (with CB or S) with greater aYS tend to have lesser, albeit still positive EaY while those with lesser aYM tend to have greater EaY.

Interestingly, EaB is the mechanical metric most sensitive to weathering, particularly in the case of the reference specimens. Clearly, an embrittling effect is present, most notably in the 0CC (WL and REF) and 30CC (REF) specimens. More broadly, as this is the only of the metrics to be primarily affected, in ductile cases, by late-stage plastic deformation which equates to first fragmentation and then disentanglement,[39–45] it is indicative of the effects of weathering on those processes. The 3.6CB/0CC/0.5S REF specimens are the clearest examples of specimens maintaining ductile failure throughout, and these specimens exhibit increasing EaB with weathering.

In general, the 3.6CB/0CC/0.5S specimens are least affected by degradation, which is to be expected from theory given their high levels of S and CB, as well as the absence of CC that may induce processing degradation. WL specimens of this material, in terms of EaB, are substantially affected by weathering, showing a sharp decrease in aEaB with increasing weathering. The presence of this effect and its absence in the REF specimens suggest a definite shift in the late-stage deformation of these specimens as a result of degradation in the weldline region. This shift, in the absence of changes to the strength at break (Figure A6A,B) would suggest similar resistance to fragmentation and disentanglement, but a reduced scope for this to occur—lending further credence to the idea of chain scission.

5 | CONCLUSIONS

Despite the complexity of the results obtained through this study, it is clear that the addition of traditional stabilizing additives such as HALS, secondary stabilizers and carbon black have positive influences on the weathering resistance of HDPE specimens taken as a function of weathering time, across chemical and mechanical measures. Calcium carbonate, broadly, may also improve the weathering resistance of these materials. In terms of the mechanical properties of the specimens, a notable synergism was found between CC and S—likely resulting from the stabilizer countering processing degradation in these more sensitive materials. Outside of that, negative interactive and squared effects were observed, suggesting that the effectivity of the additives is reduced in larger quantities and in mixed systems. It was also found that, once "stabilization" has been achieved, the additive loadings have more subtle but complex effects on the mechanical behavior of the aged specimens.

As may be anticipated, the exposed surfaces of the specimens experienced more significant degradation than those unexposed when measured as carbonyl index. In the case of the translucent materials, a slight lag can be seen, while the opaque materials exhibit more significant differences. This could not be definitively shown in terms of the double-bond or carbonate indexes.

Differences could be found between the specimens as a function of the presence or absence of weld lines. Specimens with weld lines typically exhibited increased degradation measured as carbonyl and double-bond indexes. A significant difference was also found in the front-side carbonate indexes of the WL and REF specimens, suggesting that calcium carbonate is distributed differently through the specimens as a function of the mold used.

Differences can be seen in the development of degradation products, particularly in terms of the double-bond index, as a function of formulation, with a much broader double-bond profile developing in the materials with CB (and the accompanying SEBS). In agreement with the findings of Gryn'ova et al.[2] in terms of the auto-oxidative pathway, a significant increase in carbonyl index can be seen to correspond with this increase in double-bond index in relevant materials.

The mechanical properties of the WL and REF specimens developed similarly with aging, with the exception of a switch to brittle failure in the 30CC REF specimens.

It was found that models making use of carbonyl indexes possessed more predictive power than those only taking weathering time as input, pointing towards the complexity of the degradation process and its effects on the mechanical behavior of specimens.

Future work could make use of a higher ATR-FTIR resolution, such as 2 or even 1 cm^{-1}, to allow for improved peak resolution and, thereby, fitting. This would allow the effects of specific degradation products on the bulk properties to be probed. The software written for this work may be used directly. A larger number of

specimens, perhaps enabled by a considered reduction in the number of formulations, may allow for the refinement of findings comparing specimen and weathering types in future works, as this would allow for the distribution of outcomes to better be estimated—at the cost of insight into the formulational effects. The surface effects of weathering, particularly those stemming from the leaching of calcium carbonate, must be carefully investigated for the formation of pores, for example, in which dirt or microorganisms could take a hold.

ACKNOWLEDGMENTS

The authors would like to thank their colleagues at the University of Pretoria and the Leibniz-Institut für Polymerforschung Dresden e. V. Particularly, they would like to thank Frieder Pursche and Christian Lehmann for their assistance in processing of the samples, Holger Scheibner for his assistance in mechanical characterization, and Ivonne Hasselhorst for her assistance with FTIR spectroscopy. Further thanks are due to Omya of Oftringen, Switzerland, and Caparol Industrial Solutions of Grimma-Nerchau, Germany, for the materials that they provided.

CONFLICT OF INTEREST STATEMENT

The authors declare no conflicts of interest.

DATA AVAILABILITY STATEMENT

The data that support the findings of this study are available from the corresponding author upon reasonable request.

ORCID

David Viljoen https://orcid.org/0000-0001-8252-9781
Johan Labuschagné https://orcid.org/0000-0002-4820-4585
Ines Kuehnert https://orcid.org/0000-0002-3795-3265

REFERENCES

[1] M. Tolinski, *Additives for polyolefins: getting the most out of polypropylene, polyethylene and TPO*, William Andrew, Oxford **2015**.
[2] G. Gryn'ova, J. L. Hodgson, M. L. Coote, *Org. Biomol. Chem.* **2011**, *9*, 480.
[3] J. Bolland, *Proc. R. Soc. Lond. Ser A. Math. Phys. Sci.* **1946**, *186*, 218.
[4] J. Bolland, G. Gee, *Trans. Faraday Soc.* **1946**, *42*, 236.
[5] J. Bolland, G. Gee, *Trans. Faraday Soc.* **1946**, *42*, 244.
[6] D. Feldman, *J. Polym. Environ.* **2002**, *10*, 163.
[7] L. W. McKeen, *The effect of UV light and weather on plastics and elastomers*, William Andrew, Oxford **2019**.
[8] D. Briassoulis, A. Aristopoulou, M. Bonora, I. Verlodt, *Biosyst. Eng.* **2004**, *88*, 131.
[9] J. Peña, N. Allen, M. Edge, C. Liauw, B. Valange, *Polym. Degrad. Stab.* **2001**, *72*, 259.
[10] J. C. Bart, *Additives in polymers: industrial analysis and applications*, John Wiley & Sons, England **2005**.
[11] G. Wypych, *Handbook of fillers*, 4th ed., ChemTec Publishing, Toronto **2016**.
[12] A. Valadez-Gonzalez, J. Cervantes-Uc, L. Veleva, *Polym. Degrad. Stab.* **1999**, *63*, 253.
[13] A. Valadez-Gonzalez, L. Veleva, *Polym. Degrad. Stab.* **2004**, *83*, 139.
[14] Y. Spörer, C. Blanco, M. Zimmermann, M. Berger, I. Kuehnert, *AIP Conference Proceedings*, Vol. 2055, AIP Publishing LLC, New York **2019**, p. 70002.
[15] D. Viljoen, M. Fischer, I. Kühnert, J. Labuschagné, *Polymer* **2021**, *13*, 527.
[16] R. Tocchetto, L. Barros, M. Rabello, J. D'Almeida. in Int. Mob. Technol. Conf. Exhib. **1999** 1999-01-3005.
[17] J. Almond, P. Sugumaar, M. N. Wenzel, G. Hill, C. Wallis, *E-Polymers* **2020**, *20*, 369.
[18] A. Esmaeili, A. A. Pourbabaee, H. A. Alikhani, F. Shabani, L. Kumar, *Biorem. J.* **2014**, *18*, 213.
[19] W. D. Viljoen, F. J. W. J. Labuschagne, *Polym. Test.* **2020**, *85*, 106424.
[20] S. Seabold, J. Perktold, *Proceedings of the 9th Python in Science Conference, Austin, TX*, Vol. 57, SciPy Conferences **2010**, p. 10.
[21] G. Fleissner, W. Hage, A. Hallbrucker, E. Mayer, *Appl. Spectrosc.* **1996**, *50*, 1235.
[22] C. R. Harris, K. J. Millman, S. J. Van Der Walt, R. Gommers, P. Virtanen, D. Cournapeau, E. Wieser, J. Taylor, S. Berg, N. J. Smith, R. Kern, *Nature* **2020**, *585*, 357.
[23] P. Virtanen, R. Gommers, T. E. Oliphant, M. Haberland, T. Reddy, D. Cournapeau, E. Burovski, P. Peterson, W. Weckesser, J. Bright, S. J. van der Walt, M. Brett, J. Wilson, K. J. Millman, N. Mayorov, A. R. J. Nelson, E. Jones, R. Kern, E. Larson, C. J. Carey, İ. Polat, Y. Feng, E. W. Moore, J. Van der Plas, D. Laxalde, J. Perktold, R. Cimrman, I. Henriksen, E. A. Quintero, C. R. Harris, A. M. Archibald, A. H. Ribeiro, F. Pedregosa, P. van Mulbregt, SciPy 1.0 Contributors, A. Vijaykumar, A. P. Bardelli, A. Rothberg, A. Hilboll, A. Kloeckner, A. Scopatz, A. Lee, A. Rokem, C. N. Woods, C. Fulton, C. Masson, C. Häggström, C. Fitzgerald, D. A. Nicholson, D. R. Hagen, D. V. Pasechnik, E. Olivetti, E. Martin, E. Wieser, F. Silva, F. Lenders, F. Wilhelm, G. Young, G. A. Price, G. L. Ingold, G. E. Allen, G. R. Lee, H. Audren, I. Probst, J. P. Dietrich, J. Silterra, J. T. Webber, J. Slavič, J. Nothman, J. Buchner, J. Kulick, J. L. Schönberger, J. V. de Miranda Cardoso, J. Reimer, J. Harrington, J. L. C. Rodríguez, J. Nunez-Iglesias, J. Kuczynski, K. Tritz, M. Thoma, M. Newville, M. Kümmerer, M. Bolingbroke, M. Tartre, M. Pak, N. J. Smith, N. Nowaczyk, N. Shebanov, O. Pavlyk, P. A. Brodtkorb, P. Lee, R. T. McGibbon, R. Feldbauer, S. Lewis, S. Tygier, S. Sievert, S. Vigna, S. Peterson, S. More, T. Pudlik, T. Oshima, T. J. Pingel, T. P. Robitaille, T. Spura, T. R. Jones, T. Cera, T. Leslie, T. Zito, T. Krauss, U. Upadhyay, Y. O. Halchenko, Y. Vázquez-Baeza, *Nat. Methods* **2020**, *17*, 261.
[24] M. Salvalaggio, R. Bagatin, M. Fornaroli, S. Fanutti, S. Palmery, E. Battistel, *Polym. Degrad. Stab.* **2006**, *91*, 2775.
[25] W. Yagoubi, A. Abdelhafidi, M. Sebaa, S. Chabira, *Polym. Test.* **2015**, *44*, 37.

[26] F. M. Rugg, J. J. Smith, R. C. Bacon, *J. Polym. Sci.* **1954**, *13*, 535.
[27] M. Żenkiewicz, M. Rauchfleisz, J. Czupryńska, J. Polański, T. Karasiewicz, W. Engelgard, *Appl. Surf. Sci.* **2007**, *253*, 8992.
[28] N. Jin, Y. Song, R. Ma, J. Li, G. Li, D. Zhang, *Anal. Chim. Acta* **2022**, *1197*, 339519.
[29] H. Hinsken, S. Moss, J.-R. Pauquet, H. Zweifel, *Polym. Degrad. Stab.* **1991**, *34*, 279.
[30] T. Kuroki, T. Sawaguchi, S. Niikuni, T. Ikemura, *J. Polym. Sci., Polym. Chem. Ed.* **1983**, *21*, 703.
[31] E. Mitri, L. Millucci, L. Merolle, G. Bernardini, L. Vaccari, A. Gianoncelli, A. Santucci, *Biochimica et Biophysica Acta (BBA)-General Subjects* **2017**, *1861*, 1000.
[32] Y. Hernández, T. Lozano, A. B. Morales-Cepeda, F. Navarro-Pardo, M. E. Angeles, L. Morales-Zamudio, J. A. Melo-Banda, S. Sánchez-Valdes, G. Martnez-Colunga, F. Rodrguez, *Polym. Eng. Sci.* **2019**, *59*, E279.
[33] M. Gilbert, I. Sutherland, A. Guest, *J. Mater. Sci.* **2000**, *35*, 391.
[34] D20 Committee. Tech. Rep., ASTM International, West Conshohocken, PA. **2016**.
[35] R. Satoto, W. S. Subowo, R. Yusiasih, Y. Takane, Y. Watanabe, T. Hatakeyama, *Polym. Degrad. Stab.* **1997**, *56*, 275.
[36] A. Fairbrother, H.-C. Hsueh, J. H. Kim, D. Jacobs, L. Perry, D. Goodwin, C. White, S. Watson, L.-P. Sung, *Polym. Degrad. Stab.* **2019**, *165*, 153.
[37] A. K. Sahu, K. Sudhakar, *J. Mater. Res. Technol.* **2019**, *8*, 147.
[38] S. Luzuriaga, J. Kovářová, I. Fortelný, *Polym. Degrad. Stab.* **2006**, *91*, 1226.
[39] R. Hiss, S. Hobeika, C. Lynn, G. Strobl, *J. Macromol. Sci. – Phys.* **1999**, *38*, 847.
[40] R. Hiss, S. Hobeika, C. Lynn, G. Strobl, *Macromolecules* **1999**, *32*, 4390.
[41] S. Hobeika, Y. Men, G. Strobl, *Macromolecules* **2000**, *33*, 1827.
[42] Q. Fu, Y. Men, G. Strobl, *Polymer* **2003**, *44*, 1927.
[43] Y. Men, J. Rieger, G. Strobl, *Phys. Rev. Lett.* **2003**, *91*, 095502.
[44] K. Hong, G. Strobl, *Macromolecules* **2006**, *39*, 268.
[45] L. Farge, J. Boisse, J. Dillet, S. André, P.-A. Albouy, F. Meneau, *J. Polym. Sci. B Polym. Phys.* **2015**, *53*, 1470.

SUPPORTING INFORMATION

Additional supporting information can be found online in the Supporting Information section at the end of this article.

How to cite this article: D. Viljoen, J. Labuschagné, I. Kuehnert, *J. Polym. Sci.* **2023**, *61*(16), 1912. https://doi.org/10.1002/pol.20230109